ISSN 1573-160X, *PHYSICAL OCEANOGRAPHY*, Vol. 33, Iss. 4, pp. 675-689 (2026)

Original article

Variability of the Blue Colour Index in AERONET-OC and Satellite Ocean Colour Data

E. B. Shybanov ✉, A. S. Papkova

Marine Hydrophysical Institute of RAS, Sevastopol, Russian Federation

✉ *e-shybanov@mail.ru*

Abstract

Purpose. This article discusses the use of the blue colour index in atmospheric correction for remote sensing instruments. The blue colour index is defined as the ratio of remote sensing reflectance in two shortwave channels: $CI(412/443) = R_{rs}(412)/R_{rs}(443)$. Previously, the constancy of this index was confirmed for the Black Sea. In this study, using a long-term global dataset from AERONET-OC (AErosol RObotic NETwork-Ocean Color) stations, we show that this pattern holds across other water bodies regardless of their bio-optical characteristics. The purpose of this study is to analyse the global variability of *CI*(412/443) using all available AERONET-OC *in situ* data, to develop a method for minimising polarization-induced biases in its estimation, and to evaluate the consistency of satellite-derived *CI* values from major ocean colour scanners (MODIS, VIIRS, OLCI) against the corrected *in situ* reference.

Methods and Results. We analyse $R_{rs}(412)$, $R_{rs}(443)$ and their ratios obtained from AERONET-OC data. To improve the reliability of *in situ* data, we introduce a quantitative factor dependent on solar and viewing angles, which characterises the influence of sky polarisation on the sea surface reflectivity. A systematic underestimation of the blue colour index calculated from raw AERONET-OC data is revealed. Without accounting for viewing geometry and the degree of polarisation of skylight, the systematic error in *CI* can reach 0.1–0.2. Due to measurement errors in the shortwave region at low $R_{rs}(412)$, raw AERONET-OC data overestimate the natural variability of the blue colour index. We estimate the maximum possible standard deviation of *CI* caused solely by variability in the optical properties of seawater to be 0.109. Satellite-derived *CI*(412/443) values at AERONET-OC station coordinates are also analysed. For all satellite sensors except Sentinel-3B OLCI, satellite *CI* values show high RMSD values, sometimes exceeding 0.4. In general, average *CI*(412/443) values from satellite data and *in situ* measurements show moderate agreement, although notable discrepancies exist for certain sensors and stations.

Conclusions. Our study has shown that the variability of the blue colour index across all AERONET-OC coastal stations should be significantly smaller than the variability estimated from *in situ* and satellite measurements. For most ocean colour scanners, variations in the blue colour index significantly exceed the expected variability. The results obtained have important practical applications for the creation and further development of regional algorithms for atmospheric correction.

Keywords: remote ocean colour, remote-sensing reflectance, blue colour index, atmospheric correction, skylight polarisation, AERONET-OC, satellite validation

Acknowledgments: The study was conducted under State Assignment No. FNNN-2024-0012 and funded by FSBSI FSC MHI. The assignment is entitled “Analysis, Diagnosis and Operational Forecast of the State of Hydrophysical and Hydrochemical Fields of Marine Waters Based on Mathematical Modeling Using the Data of Remote and Contact Measurement Methods”.

For citation: Shybanov, E.B. and Papkova, A.S., 2026. Variability of the Blue Colour Index in AERONET-OC and Satellite Ocean Colour Data. *Physical Oceanography*, 33(4), pp. 675-689.

Introduction

Remote sensing reflectance, $R_{rs}(\lambda)$, is an essential input parameter for calculating a number of bio-optical parameters. It is known that $R_{rs}(\lambda)$ data often have abnormally low or even negative values in the shortwave ("blue") spectral region, regardless of the satellite used and the study area, indicating poor-quality atmospheric correction. This problem is common in coastal and inland water bodies, usually related to Case 2 waters [1–7], and can be explained by a combination of hydro-optical and atmospheric factors. Thus, $R_{rs}(\lambda)$ values, influenced by large variations in the concentrations of optically active constituents, may be significantly reduced due to light absorption by non-living organic matter. As the relative contribution of the atmospheric component increases, inadequate accounting for atmospheric aerosols – including mineral dust, smog, industrial aerosols and even fine background aerosols – can result in poor-quality satellite products [8–14].

The problem of poor-quality $R_{rs}(\lambda)$ data in the blue bands is not limited to the Black Sea but has been documented globally. The authors in [15] demonstrated across more than 1,000 matchups from lakes, rivers, and coastal waters that the largest atmospheric correction uncertainties (25–60%) consistently occur at 412–443 nm. The authors in [7] developed a spectral-shape algorithm to recover $R_{rs}(412)$ and $R_{rs}(443)$ from global SeaWiFS, MODIS, and VIIRS data, confirming that blue-band uncertainties are a universal challenge for ocean colour remote sensing. The proportion of scattered radiation also increases with increasing solar zenith and viewing angles, particularly at temperate and polar latitudes [16].

A number of studies have shown that incorporating information from the "blue" spectral region into standard approaches (e.g., the approach of Gordon and Wang [17]) improves the quality of remote sensing data. Remote sensing reflectance in the shortwave region can be used to construct a fundamentally new atmospheric correction algorithm based on interpolation methods, as demonstrated for the Black Sea [18–19]. To implement such an atmospheric correction procedure, it is necessary to specify a constraint for the value of the remote sensing reflectance in the shortwave region. In [20], the concept of the "blue" colour index was introduced to determine the upwelling radiation signal in the shortwave region from remote sensing data. The "blue" colour index is defined as the ratio of remote sensing reflectance in two channels in the shortwave region, for example, $R_{rs}(412)/R_{rs}(443)$ (hereinafter $CI(412/443)$).

The concept of using $CI(412/443)$ as a relatively stable optical characteristic is supported by observations from various marine regions. For the oligotrophic waters of the Mediterranean Sea, it was shown that elevated CDOM absorption reduces the overall "blueness", while the relationship between the blue bands remains regionally consistent, with $CI(412/443)$ varying between 0.8 and 1.1 [21]. In the optically complex Arctic waters of the Beaufort Sea, CDOM dominance was reported to result in extremely low $R_{rs}(\lambda)$ values in the blue spectral region [22], highlighting the need for stable blue-band references for atmospheric correction. Analysis of global bio-optical data from NOMAD (NASA bio-Optical Marine Algorithm Data) indicates that $CI(412/443)$ typically falls within the range of 0.65–

1.2 [23]. A value of 1.2 ± 0.2 has also been reported for Case 1 waters [24]. Further evidence comes from observations in the Red Sea, where seasonal variation in *CI*(412/443), ranging from 0.6 to 1.1 and associated with spring phytoplankton blooms, was reported [25]. This example shows that, despite its overall stability, the index may exhibit a seasonal cycle. It has been reported in [26] that blue-band uncertainties dominate satellite validation errors across European seas, with certain regions (e.g., the South-East Mediterranean and the Atlantic Ocean) being underrepresented in AERONET-OC (AErosol RObotic NETwork-Ocean Color) data. An analysis of the long-term *in situ* dataset from AERONET stations and shipborne measurements by MHI RAS showed that the values of the "blue" colour index for the coastal waters of the Black Sea varied only slightly. The optimal values of *CI*(412/443) for the Black Sea are in the range of 0.77–0.80. These values were derived from long-term *in situ* measurements by MHI RAS and correspond to the typical bio-optical conditions of the Black Sea coastal waters, where CDOM absorption dominates over chlorophyll *a* absorption in the blue spectral region [20].

The broad potential applications of the "blue" colour index for a number of oceanographic tasks, demonstrated for the Black Sea [18–20], indicate the need to investigate its variability in other water bodies. The analysis includes not only coastal stations (Case 2 waters) but also stations in the open ocean (Case 1 waters). Since skylight is partially polarised and the AERONET-OC processing protocol does not account for this, systematic errors in $R_{rs}(412)$ and $R_{rs}(443)$ can occur, particularly in the blue spectral region where water-leaving radiance is low [27]. A detailed description of the correction method is given in the next Section.

In addition to the *in situ* data, this paper presents an analysis of *CI*(412/443) value at the locations of the AERONET-OC stations under study, derived from the available ocean colour sensors: MODIS on board Aqua/Terra, VIIRS on board SNPP, and OLCI on board Sentinel 3A/3B. The comparison of satellite and *in situ* measurements allows the agreement and accuracy of data obtained using different remote sensing instruments to be assessed. The potential applications of this study include the development of new regional algorithms based on the assumption of the constancy of the "blue" colour index in the studied areas, the use of the existing algorithm for additional correction proposed in [18], and the development of a completely new approach to atmospheric correction using Level-1 data, as proposed in [19].

Despite the demonstrated utility of the blue colour index for atmospheric correction in the Black Sea, its global variability remains poorly quantified, and the influence of skylight polarization on *in situ CI* estimates has not been systematically addressed. Moreover, a comprehensive cross-comparison of *CI* retrievals from major ocean colour sensors (MODIS, VIIRS, OLCI) against a unified *in situ* reference is lacking. This study fills these gaps by (1) developing a simple correction for polarisation-induced biases in AERONET-OC data, (2) establishing the global range and natural variability of *CI*(412/443), and (3) providing the first multi-sensor assessment of satellite-derived *CI* against corrected *in situ* measurements.

The aim of this paper is to analyse the global variability of *CI*(412/443) using all available AERONET-OC *in situ* data, to develop a method for minimising polarization-induced biases in its estimation, and to evaluate the consistency of satellite-derived *CI* values from the MODIS, VIIRS and OLCI ocean colour sensors with the corrected *in situ* reference data.

Materials and methods

The main source of *in situ* data was the AERONET-OC measurements. The AERONET network of land-based CIMEL-318 photometers was originally designed for atmospheric studies, but was later extended to support marine applications. AERONET-OC provides measurements of water-leaving radiance following standardised protocols [28]. In this study, we used Level-2 remote sensing reflectance data from all 38 AERONET-OC stations (including successor stations). The data cover the entire available period for each station, from the start of operations (the earliest being 2002 for AAOT) to 2025. For satellite data from SeaBASS, the match-ups were selected over the same temporal range (2002–2025) with a ±3-hour window around each *in situ* measurement. Fig. 1 shows the spatial coverage of the *in situ* measurements.

F i g. 1. Locations of the AERONET-OC stations used in this study (source: https://aeronet.gsfc.nasa.gov)

The distribution of stations is uneven, with the largest number located near North American and European waters. The full list of stations is available on the AERONET-OC website. Four stations are located in clear oceanic waters (Case 1). The data include remote sensing reflectance values obtained with CIMEL CE-318 photometers. Over the long-term operation of the AERONET-OC network, several stations have been decommissioned and replaced by successor stations to ensure data continuity. Specifically, the AAOT station in the Mediterranean Sea was replaced by Venice; the USC_SEAPRISM station in the Pacific Ocean was replaced by USC_SEAPRISM2; and the Gloria station in the Black Sea was replaced by Section-7_Platform. In this study, data from both the original stations and their successors were treated as belonging to the same time series, given their close proximity and the use of identical measurement protocols. This approach maximises the temporal coverage while maintaining consistency across the record. The remote sensing reflectance is calculated as $R_{rs}(\lambda) = L_{wn}(\lambda)/F_o(\lambda)$, where $L_{wn}(\lambda)$ is the normalised water-leaving radiance and $F_o(\lambda)$ is the extraterrestrial solar irradiance. The AERONET-OC network provides $L_{wn}(\lambda)$ data at Levels 1.5 and 2. All data are publicly available and accessible on https://aeronet.gsfc.nasa.gov/.

A simple method for minimising polarization effects when calculating average colour index values using AERONET-OC data

Minimising polarisation effects is necessary to reduce bias in *CI*(412/443) estimates from AERONET-OC data. Because the AERONET-OC processing protocol does not account for skylight polarisation, systematic errors occur – especially for shortwave channels where water-leaving radiance is low. These errors affect $R_{rs}(412)$ more strongly than $R_{rs}(443)$, thereby biasing *CI*(412/443). By quantifying the dependence of *CI* on $\cos 2\alpha$, we account for this bias and estimate the corrected *CI* value at $\cos 2\alpha = 0$. This corrected *CI* is then used as a reference for evaluating satellite data. The measurement protocol uses a viewing angle of 140° and an azimuth offset of ±90° relative to the Sun. Fig. 2 shows the reflection geometry of atmospherically scattered light during measurements of sea-surface reflectance.

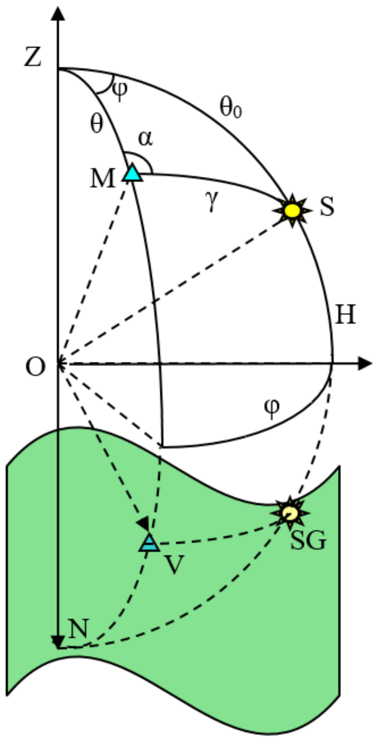

F i g. 2. Geometry of the reflection of scattered skylight during sea-surface reflectance measurements. O – observer position; Z – zenith; N – nadir; V – observation point on the sea surface; M – point in the sky from which scattered light enters the instrument after specular reflection from the sea surface; S – the Sun; SG – sun glint; θ_0 – solar zenith angle; θ – viewing zenith angle; φ – relative azimuth angle between the solar and viewing azimuths; α – angle between the scattering plane and the observation plane; γ – scattering angle

The geometry shown in Fig.2 is used to calculate the reflected component. The viewing plane passes through points Z, M, O; the solar vertical plane passes through points Z, S, O; and the scattering plane passes through points M, O, S. Points Z, S, M form a spherical triangle in which the angle α between the scattering plane and the observation plane affects the reflection coefficient of polarised light. The degree of polarisation of scattered light is defined as $P_a = (L_\perp - L_{II})/(L_\perp + L_{II})$, where $L_\perp$ and L_{II} are the perpendicular and parallel components of scattered radiation. The polarized component is reflected according to the two Fresnel coefficients $R_\perp$ and R_{II} as follows: $R_\perp \cos^2 \alpha + R_{II} \sin^2 \alpha$. The unpolarised component is reflected with the mean Fresnel coefficient $R_f = (R_\perp + R_{II})/2$ and is weighted by the coefficient $(1 - P_a)$. Since $2\cos^2 \alpha - 1 = 1 - 2\sin^2 \alpha = \cos 2\alpha$, the resulting reflection coefficient is given by:

$$R_p = P_a(R_\perp \cos^2\alpha + R_{II}\sin^2\alpha) + (1 - P_a)(R_\perp + R_{II})/2 = \\ = R_f(1 + P_f P_a \cos 2\alpha), \quad (1)$$

where $P_f = (R_\perp - R_{II})/(R_\perp + R_{II})$ is the degree of polarisation arising from reflection at the surface.

In the spherical triangle ZSM, arc ZS represents the solar zenith angle θ_0, arc ZM represents the viewing zenith angle θ, and arc SM represents the scattering angle γ. The azimuth angle φ is the difference between the solar azimuth and the viewing azimuth, i.e. the angle between the arcs ZS and ZM. According to the sine rule, $\sin\alpha/\sin\theta_0 = \sin\varphi/\sin\gamma$. The scattering angle is given by $\cos\gamma = \cos\theta_0 \cos\theta + \sin\theta_0 \sin\theta\cos\varphi$, hence:

$$\cos 2\alpha = 1 - \frac{2\sin^2\theta_0 \sin^2\varphi}{1 - (\cos\theta_0\cos\theta + \sin\theta_0 \sin\theta\cos\varphi)^2}.$$

The AERONET sensor observes the sea surface at a viewing angle of 40° and an azimuthal angle of 90° relative to the Sun. Under these conditions, $P_f = 0.761$, and the factor in parentheses in equation (1) for a viewing angle of 40° is given by:

$$1 + 0.761 \cdot P_a \left(1 - \frac{2\cos^2 h_0}{1 - 0.587\sin^2 h_0}\right),$$

where h_0 is the solar elevation angle.

At cos 2α = 0, the polarisation-dependent term vanishes. By quantifying the dependence of *CI* on cos 2α, we accounted for this bias. For each station, the *CI*(412/443) values were plotted against cos 2α, and an approximation function was fitted. The corrected value of *CI* was taken as the value of this function at cos 2α = 0. If no data were available at cos 2α > 0, the corrected value of *CI* was taken as the value of the approximation function at the available cos 2α value closest to zero. The RMSD was calculated relative to the approximation function. When the central wavelengths of a given instrument deviated from the nominal wavelengths of 412 nm and 443 nm by up to 3 nm, *CI*(412/443) was recalculated using linear interpolation to the nominal wavelengths based on instrument-specific calibration data. In particular, for each measurement, we identified the actual central wavelengths λ_1 and λ_2 closest to 412 nm and 443 nm, respectively, using the calibration coefficients provided for each CIMEL-318 photometer. The remote sensing reflectance $R_{rs}(\lambda_1)$ and $R_{rs}(\lambda_2)$ were then linearly interpolated to the nominal wavelengths 412 nm and 443 nm before computing *CI*(412/443).

Remote sensing data from SeaBASS

We used data from SeaBASS, the official ocean colour validation database, [29], which provides synchronised pairs of *in situ* and satellite measurements. Satellite measurements were obtained from a 5×5-pixel window centred on the *in situ* location, with standard quality flags applied. We used data from MODIS aboard Aqua/Terra, VIIRS aboard SNPP, and OLCI aboard Sentinel 3A/3B at the locations of AERONET-OC stations. Of the 38 AERONET-OC stations described above, 29 had sufficient high-quality satellite match-ups in the SeaBASS database. For the remaining 9 stations, co-located satellite data were either unavailable or excluded because they did not meet the quality-control criteria. All satellite data are publicly available from the SeaBASS website: https://seabass.gsfc.nasa.gov/.

Results and discussion

To assess the variability of the blue colour index and to validate the proposed polarisation correction method, we first analysed the relationship between *CI*(412/443) and the geometric factor cos 2α for individual AERONET-OC stations. As shown in Fig. 3, the dependence of *CI* on cos 2α exhibits a clear systematic trend: the colour index increases with cos 2α for all stations, regardless of their bio-optical characteristics. This confirms that neglecting skylight polarisation introduces a systematic bias into the *in situ* estimates of *CI*. Fig. 3, *a* presents an example for the Chesapeake_Bay station, located in coastal waters of the USA. At low values of cos 2α, the AERONET-OC algorithms underestimate the colour index. The mean *CI* value of 0.723 differs from the fitted value at cos 2α = 0 (*CI* = 0.826). Figs. 3, *b* and 3, *c* show *CI* data at AAOT (Venice Tower) in the Mediterranean Sea and at ARIAKE_TOWER in Japan, where the mean $R_{rs}(412)$ values (> 0.0076 and > 0.0079, respectively) are higher than that at Chesapeake_Bay, and the slope of the dependence of *CI* on cos 2α is less pronounced. Finally, Fig. 3, *d* shows the results for the Palgrunden station in the Baltic Sea, which exhibits the lowest water-leaving reflectance among all AERONET-OC stations. Here, despite the weak correlation, the approximation function shows a similar pattern, while the correction is more significant. This station, like other stations with low $R_{rs}(412)$ values, represents an extreme case where accurate correction for polarisation effects is essential for reliable *CI* estimation.

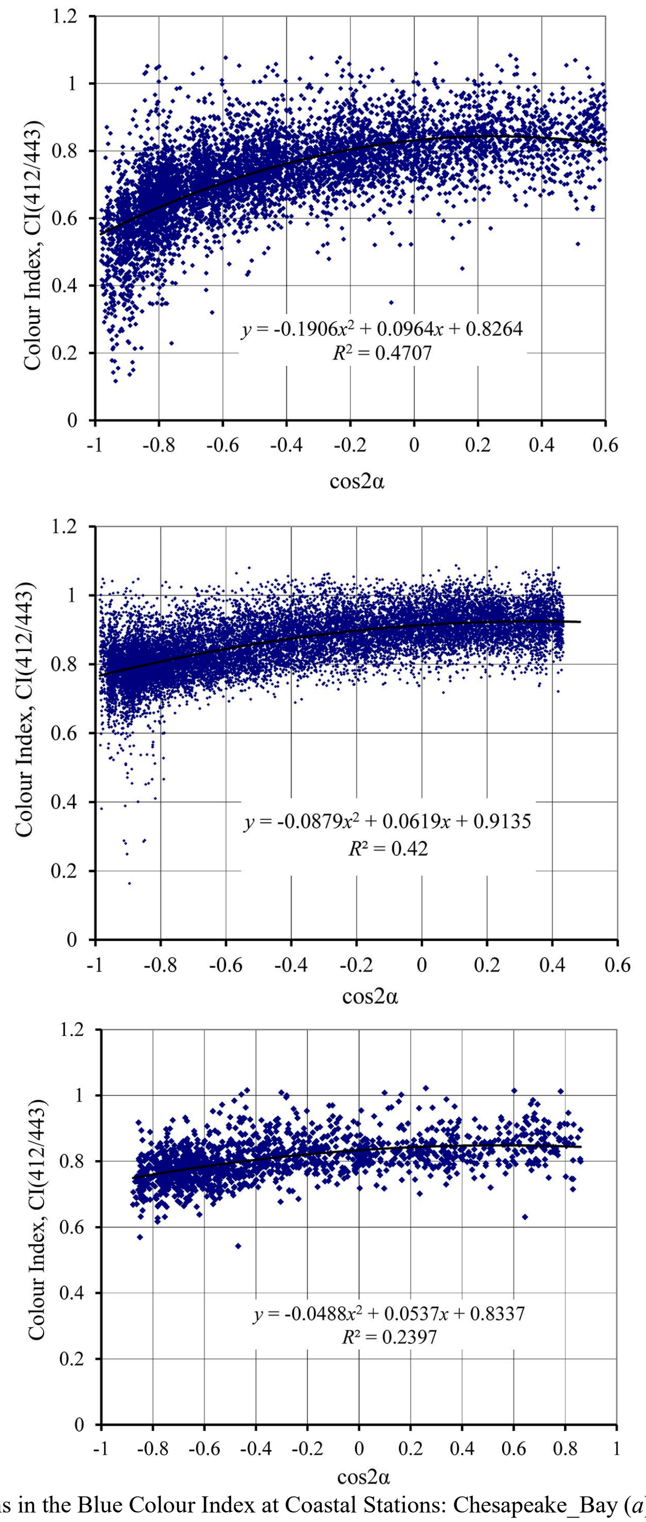

F i g. 3. Variations in the Blue Colour Index at Coastal Stations: Chesapeake_Bay (*a*), AAOT (Venice Tower) (*b*), ARIAKE_TOWER (*c*), Palgrunden (*d*)

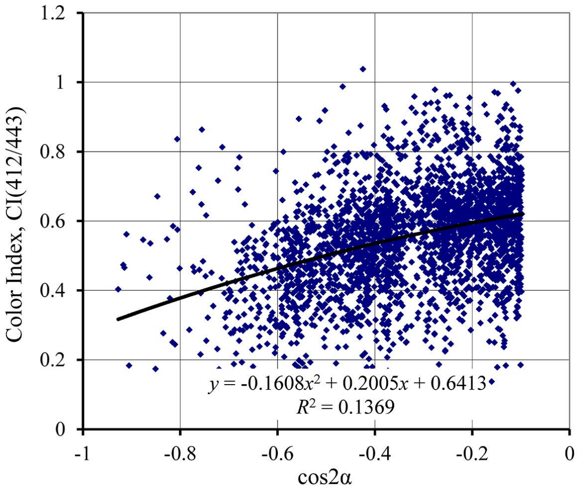

F i g. 3. (Continued)

The systematic dependence of *CI*(412/443) on cos 2α observed in Fig. 3 was not limited to the four stations shown but was also found throughout the analysed AERONET-OC dataset.

Table 1 summarises the corrected *CI*(412/443) values along with the corresponding reflectance $R_{rs}(412)$ for all 38 stations, sorted in ascending order of *CI*. These data allow us to quantify the range of the blue colour index across the analysed stations and to assess the influence of the optical properties of water on its variability. λ^{MAX} characterises the optical properties of water with respect to the concentration of dissolved organic matter. For clear oceanic waters, λ^{MAX} typically lies in the range of approximately 440–470 nm, whereas for high-CDOM waters (usually coastal), it is higher than 500 nm.

T a b l e 1

Statistical characteristics (mean *CI*(412/443) ± RMSD and reflectance R_{rs}(412)) for the AERONET-OC stations after accounting for polarisation effects

Station	Coordinates	*CI*(412/443)	R_{rs}(412), sr^{-1}	λ^{MAX}, nm
Palgrunden	58.755°N, 13.152°E	0.620 ± 0.135	0.00073	555
Sacramento River	38.050°N, 121.888°W	0.645 ± 0.021	0.00403	551
Banana RIVER	28.367°N, 80.633°W	0.680 ± 0.116	0.00129	560
Grizzly Bay	38.108°N, 122.056°W	0.718 ± 0.037	0.00745	560
Helsinki_Lighthouse	59.949°N, 24.926°E	0.734 ± 0.191	0.00054	555
Gustav_Dalen_Tower	58.594°N, 17.467°E	0.751 ± 0.151	0.00085	555
Lake_Okeechobee N	27.139°N, 80.789°W	0.778 ± 0.078	0.0018	710
LISCO	40.955°N, 73.342°W	0.779 ± 0.101	0.00141	550
Lucinda	18.520°S, 146.388°E	0.780 ± 0.074	0.00737	551
Zeebrugge-MOW1	51.362°N, 3.120°E	0.785 ± 0.060	0.00893	531

Table 1. (Continued)

Station	Coordinates	*CI*(412/443)	R_{rs}(412), sr^{-1}	λ^{MAX}, nm
Leodo_Station	32.123°N, 125.182°E	0.804 ± 0.061	0.00796	532
Galata_Platform	43.045°N, 28.193°E	0.805 ± 0.068	0.00301	490
Irbe_Lighthouse	57.751°N, 21.723E	0.806 ± 0.130	0.00113	560
Gloria	44.600N, 29.360°E	0.818 ± 0.089	0.00266	555
Chesapeake_Bay	39.124°N, 28.193°W	0.826 ± 0.059	0.00198	560
Blyth_NOAH	55.146°N, 1.421°W	0.826 ± 0.079	0.00173	532
South_Greenbay	44.598°N, 87.954°W	0.832 ± 0.083	0.00164	560
ARIAKE TOWER	33.104°N, 130.272°E	0.834 ± 0.055	0.00512	560
Bahia Blanca	39.148°S, 61.722°W	0.835 ± 0.039	0.01258	560
MVCO	41.325°N, 70.567°W	0.836 ± 0.069	0.00266	555
Lake_Okeechobee S	26.902°N, 80.789°W	0.837 ± 0.053	0.00348	710
COVE_SEAPRISM	36.900°N, 75.710°W	0.846 ± 0.132	0.00293	530
Thornton_C-power	51.532°N, 2.955°E	0.847 ± 0.106	0.00235	551
San_Marco_Platform	2.942°S, 40.215°E	0.852 ± 0.078	0.00406	560
Section7_Platform	44.546°N, 29.447°E	0.854 ± 0.083	0.00256	560
WaveCIS_Site_CSI_6	28.867°N, 90.483°W	0.867 ± 0.103	0.00226	552
Kemigawa_Offshore	35.611°N, 140.023°E	0.873 ± 0.109	0.00122	560
Gageocho Station	33.942°N, 124.593°E	0.887 ± 0.109	0.00332	532
Socheongcho	37.423°N, 124.738°E	0.902 ± 0.097	0.00326	531
Abu_Al_Bukhoosh	25.495°N, 53.146°E	0.911 ± 0.094	0.00392	490
AAOT, (Venice)	43.314°N; 12.508°E	0.913 ± 0.056	0.00477	490
Lake_Erie	41.826°N, 83.194°W	0.923 ± 0.109	0.00643	550
Venice	43.314°N, 12.508°E	0.930 ± 0.056	0.00483	490
USC_SEAPRISM 2	33.564°N, 118.118°W	1.034 ± 0.063	0.00378	490
USC_SEAPRISM 1	33.564°N, 118.118°W	1.040 ± 0.069	0.00375	412
GOT_Seaprism	9.286°N, 101.14°E	1.077 ± 0.051	0.00575	412
Casablanca_Platform	40.717°N, 1.358°E	1.128 ± 0.035	0.00738	412
Plogan_Tower	28.041°N, 15.385°W	1.218 ± 0.061	0.00613	400

Note: The stations are listed in ascending order of *CI*(412/443). Stations with successors (AAOT/Venice, USC_SEAPRISM1/USC_SEAPRISM2, Gloria/Section-7_Platform) are listed separately to preserve the original time series; their data were, however, treated as continuous records for the analysis.

Table 1 reveals three key features of the corrected blue colour index. First, *CI*(412/443) is relatively stable across most stations, with 86% of values lying between 0.75 and 0.95. Second, there is a general distinction between high-CDOM coastal waters (CI < 0.8, λ^{MAX} > 550 nm) and clear oceanic waters (CI > 1.0, λ^{MAX} < 490 nm), with transitional waters occupying the intermediate range. Third, the RMSD tends to decrease with increasing R_{rs}(412), reaching a minimum of 0.109 at R_{rs}(412) > 0.006, which we interpret as the maximum natural variability of *CI*.

The RMSD of *CI* is strongly anti-correlated with $R_{rs}(412)$: stations with very low $R_{rs}(412)$ (< 0.001) show the largest RMSD (> 0.13), which may reflect the greater contribution of instrumental noise at low signal levels. For stations with $R_{rs}(412)$ > 0.006 sr^{-1} (e.g., Grizzly_Bay, Zeebrugge-MOW1, Blyth_NOAH, Lake_Erie), the RMSD does not exceed 0.109. We therefore propose 0.109 as a conservative upper bound for the natural variability of *CI*(412/443) in the absence of significant measurement errors.

Having established the corrected *in situ CI*(412/443) values and their variability, we evaluated the agreement between the satellite-derived and corrected *in situ* estimates. Using the SeaBASS database, we calculated *CI*(412/443) from MODIS aboard Aqua/Terra, VIIRS aboard SNPP, and OLCI aboard Sentinel 3A/3B for the AERONET-OC stations that had sufficient match-ups. Despite the application of standard Sea BASS quality-control procedures, negative $R_{rs}(412)$ or $R_{rs}(443)$ values remained in the dataset. These values were removed as indicators of atmospheric correction failure; an equal number of anomalously high *CI* values were also excluded to avoid bias caused by asymmetric truncation of the distribution. Notably, despite following the seabass standard data cleaning protocols, negative values of the remote sensing reflectance were still present in the dataset. Table 2 presents the mean satellite-derived *CI*(412/443) values alongside the corrected *in situ* reference values for all available stations, listed alphabetically. This comparison allows us to assess the agreement between the estimates from each sensor and the *in situ* benchmark and to identify systematic biases in atmospheric correction.

Table 2 reveals systematic but sensor-dependent discrepancies between satellite-derived and *in situ CI*(412/443) values. For clear oceanic waters (Casablanca_Platform, USC_SEAPRISM, GOT_Seaprism), all satellite sensors yield values lower than the in situ reference, with MODIS Terra showing the largest negative bias in some cases. For high-CDOM coastal waters (Palgrunden, Helsinki_Lighthouse, Gustav_Dalen_Tower), the bias direction varies by sensor: MODIS Aqua and Terra tend to overestimate *CI*, while VIIRS SNPP often underestimates it. Sentinel 3A and Sentinel 3B show intermediate behaviour, with the latter generally providing closer agreement with *in situ* measurements.

The RMSD of satellite-derived *CI* varies widely across stations and sensors. While many MODIS and VIIRS retrievals exhibit RMSD values exceeding the proposed natural variability limit of 0.109, several stations (e.g., Bahia_Blanca, Lucinda, Zeebrugge-MOW1) show RMSD below this threshold, particularly for OLCI sensors. Overall, Sentinel 3B OLCI demonstrates the most consistent performance, with the smallest RMSD and the closest mean *CI* values to the *in situ* reference across the majority of stations. Sentinel 3A shows generally higher scatter, and its bias is less systematic.

The results presented above indicate that standard atmospheric correction does not always produce consistent *CI*(412/443) values, particularly in optically complex coastal waters with low $R_{rs}(412)$. To address this issue, a correction algorithm was previously proposed in [18–19]. The algorithm uses a regionally stable value of the blue colour index, derived from in situ data such as AERONET-OC measurements, to adjust the satellite-derived remote sensing reflectance throughout the visible spectral range.

Table 2

Comparison of satellite-derived *CI*(412/443)

Station	*In situ*	Modis Aqua	Modis Terra	VIIRS SNPP	Sentinel 3A	Sentinel 3B
AAOT	0.913	0.884 ± 0.192	0.894 ± 0.169	0.800 ± 0.125	0.817 ± 0.130	0.885 ± 0.067
ARIAKE_TOWER	0.834	0.676 ± 0.307	0.689 ± 0.209	0.612 ± 0.207	0.669 ± 0.201	0.836 ± 0.060
Bahia Blanca	0.835	0.824 ± 0.046	0.850 ± 0.063	0.773 ± 0.054	0.770 ± 0.102	0.871 ± 0.036
Casablanca_Platform	1.128	1.084 ± 0.222	1.058 ± 0.159	0.949 ± 0.129	0.990 ± 0.090	1.070 ± 0.084
Chesapeake_Bay	0.826	0.768 ± 0.210	0.885 ± 0.298	0.677 ± 0.340	0.810 ± 0.313	0.739 ± 0.099
COVE_SEAPRISM	0.846	0.857 ± 0.156	0.836 ± 0.168	0.715 ± 0.103	–	–
Galata_Platform	0.805	0.810 ± 0.303	0.750 ± 0.262	0.704 ± 0.169	0.724 ± 0.195	0.791 ± 0.107
Gloria	0.818	0.740 ± 0.180	0.686 ± 0.303	0.702 ± 0.177	0.692 ± 0.198	0.838 ± 0.089
GOT_Seaprism	1.077	0.951 ± 0.170	1.070 ± 0.131	0.990 ± 0.094	–	–
Gustav_Dalen_Tower	0.751	0.974 ± 0.456	0.920 ± 0.526	0.656 ± 0.271	0.753 ± 0.264	0.783 ± 0.161
Helsinki_Lighthouse	0.734	1.059 ± 0.333	0.984 ± 0.534	0.662 ± 0.301	0.876 ± 0.234	–
Leodo_Station	0.804	–	–	0.688 ± 0.001	–	–
Irbe_Lighthouse	0.806	0.905 ± 0.422	0.931 ± 0.391	0.662 ± 0.248	0.691 ± 0.210	0.721 ± 0.167
Kemigawa_Offshore	0.873	1.216 ± 0.579	1.188 ± 0.500	0.742 ± 0.251	0.845 ± 0.205	0.710 ± 0.139
Lake_Erie	0.923	0.850 ± 0.134	0.856 ± 0.183	0.762 ± 0.139	0.762 ± 0.118	0.837 ± 0.110
Lake_Okeechobee	0.808	1.729 ± 0.644	1.660 ± 0.460	1.772 ± 0.640	1.674 ± 0.282	0.831 ± 0.056
LISCO	0.779	0.921 ± 0.522	0.810 ± 0.553	0.565 ± 0.288	0.754 ± 0.322	0.651 ± 0.133
Lucinda	0.78	0.747 ± 0.071	0.754 ± 0.069	0.656 ± 0.116	0.626 ± 0.083	0.782 ± 0.048
MVCO	0.836	0.785 ± 0.205	0.709 ± 0.238	0.621 ± 0.177	0.743 ± 0.146	0.840 ± 0.135
Palgrunden	0.620	0.721 ± 0.384	0.936 ± 0.613	0.600 ± 0.304	0.584 ± 0.240	0.574 ± 0.139
San_Marco_Platform	0.852	0.743 ± 0.132	0.875 ± 0.124	0.760 ± 0.138	0.891 ± 0.113	0.869 ± 0.071
Section7_Platform	0.854	0.872 ± 0.357	0.835 ± 0.285	0.720 ± 0.168	0.766 ± 0.179	0.829 ± 0.105
Socheongcho	0.902	0.829 ± 0.215	0.745 ± 0.179	0.741 ± 0.169	0.764 ± 0.118	0.832 ± 0.093
South_Greenbay	0.832	0.913 ± 0.794	1.684 ± 0.594	1.123 ± 0.875	1.501 ± 0.564	0.768 ± 0.091
Thornton_C-power	0.847	0.847 ± 0.150	0.790 ± 0.306	0.781 ± 0.150	0.817 ± 0.182	0.819 ± 0.113
USC_SEAPRISM	1.04	1.007 ± 0.209	0.982 ± 0.237	0.885 ± 0.144	0.925 ± 0.122	1.031 ± 0.059
Venice	0.930	0.884 ± 0.162	0.851 ± 0.192	0.774 ± 0.143	0.814 ± 0.150	0.879 ± 0.072
WaveCIS_Site_CSI_6	0.867	0.872 ± 0.217	0.833 ± 0.199	0.739 ± 0.165	0.819 ± 0.113	0.810 ± 0.137
Zeebrugge-MOW1	0.785	0.701 ± 0.102	0.697 ± 0.165	0.656 ± 0.120	0.727 ± 0.114	0.801 ± 0.081

Note: values are given as mean ± RMSD with corrected *in situ* measurements at AERONET-OC stations. *In situ* reference values are taken from Table 1. For stations with two records in Table 1 (Lake Okeechobee N/S and USC_SEAPRISM1/2), the mean value is used.

The method does not rely on assumptions specific to the Black Sea and may therefore be applicable to other marine regions, provided that the local reference *CI*(412/443) is known or can be reliably estimated from existing measurements.

Conclusions

The evaluation of satellite-derived *CI(*412/443) against the corrected *in situ* reference reveals that current atmospheric correction schemes produce estimates with considerable scatter, the magnitude and direction of which depend on both the sensor and the optical water type. MODIS Aqua, MODIS Terra, and VIIRS SNPP exhibit RMSD values that often – but not always – exceed the estimated natural variability limit of 0.109. Among the analysed sensors, Sentinel 3B OLCI shows the most consistent agreement with *in situ* measurements, with the lowest RMSD and smallest bias across most stations, while Sentinel 3A demonstrates greater variability. These findings highlight the need for improved atmospheric correction algorithms, particularly for optically complex coastal waters, and support the use of regionally stable *CI* reference values derived from polarisation-corrected *in situ* data.

REFERENCES

1. Morel, A. and Prieur, L., 1977. Analysis of Variations in Ocean Color. *Limnology and Oceanography*, 22(4), pp. 709-722. https://doi.org/10.4319/lo.1977.22.4.0709
2. Gordon, H.R., 2021. Evolution of Ocean Color Atmospheric Correction: 1970–2005. *Remote Sensing*, 13(24), 5051. https://doi.org/10.3390/rs13245051
3. Wang, M., 2007. Remote Sensing of the Ocean Contributions from Ultraviolet to Near-Infrared Using the Shortwave Infrared Bands: Simulations. *Applied Optics*, 46(9), pp. 1535-1547. https://doi.org/10.1364/AO.46.001535
4. Gordon, H.R. and Morel, A.Y., 1983. *Remote Assessment of Ocean Color for Interpretation of Satellite Visible Imagery: A Review*. Lecture Notes on Coastal and Estuarine Studies; vol. 4. New York: Springer, 114 p. https://doi.org/10.1007/978-1-4684-6280-7
5. Kuchinke, C.P., Gordon, H.R., Harding, L.W., Jr. and Voss, K.J., 2009. Spectral Optimization for Constituent Retrieval in Case 2 Waters II: Validation Study in the Chesapeake Bay. *Remote Sensing of Environment*, 113(3), pp. 610-621. https://doi.org/10.1016/j.rse.2008.11.002
6. Gross-Colzy, L., Colzy, S., Frouin, R. and Henry, P., 2007. A General Ocean Color Atmospheric Correction Scheme Based on Principal Components Analysis - Part I: Performance on Case 1 and Case 2 Waters. In: R. Frouin and Z. Lee, eds., 2007. *Proceedings of SPIE*. Tomsk, vol. 6680: Coastal Ocean Remote Sensing, 668002. https://doi.org/10.1117/12.738508
7. Wei, J., Yu, X., Lee, Z., Wang, M. and Jiang, L., 2020. Improving Low-Quality Satellite Remote Sensing Reflectance at Blue Bands over Coastal and Inland Waters. *Remote Sensing of Environment*, 250, 112029. https://doi.org/10.1016/j.rse.2020.112029
8. Kaufman, Y.J., Tanré, D. and Boucher, O., 2002. A Satellite View of Aerosols in the Climate System. *Nature*, 419(6903), pp. 215-223. https://doi.org/10.1038/nature01091
9. Suslin, V.V., Slabakova, V.K., Kalinskaya, D.V., Pryakhina, S.F. and Golovko, N.I., 2016. Optical Features of the Black Sea Aerosol and the Sea Water Upper Layer Based on In Situ and Satellite Measurements. *Physical Oceanography*, (1), pp. 20-32. https://doi.org/10.22449/1573-160X-2016-1-20-32
10. Kalinskaya, D.V. and Papkova, A.S., 2022. Why Is It Important to Consider Dust Aerosol in the Sevastopol and Black Sea Region during Remote Sensing Tasks? A Case Study. *Remote Sensing*, 14(8), 1890. https://doi.org/10.3390/rs14081890

11. Suetin, V.S. and Korolev, S.N., 2021. Application of Satellite Data for Retrieving the Light Absorption Characteristics in the Black Sea Waters. *Physical Oceanography*, 28(2), pp. 205-214. https://doi.org/10.22449/1573-160X-2021-2-205-214

12. Shybanov, E.B. and Papkova, A.S., 2022. Differences in the Ocean Color Atmospheric Correction Algorithms for Remote Sensing Reflectance Retrievals for Different Atmospheric Conditions. *Sovremennye Problemy Distantsionnogo Zondirovaniya Zemli iz Kosmosa*, 19(6), pp. 9-17. https://doi.org/10.21046/2070-7401-2022-19-6-9-17 (in Russian).

13. Song, Z., He, X., Bai, Y., Dong, X., Wang, D., Li, T., Zhu, Q. and Gong, F., 2023. Atmospheric Correction of Absorbing Aerosols for Satellite Ocean Color Remote Sensing over Coastal Waters. *Remote Sensing of Environment*, 290, 113552. https://doi.org/10.1016/j.rse.2023.113552

14. Lv, J., Feng, L. and Zhao, D., 2024. Validation of Global Gridded Aerosol Models in Inland/Coastal Water Atmospheric Correction for MODIS, VIIRS, and Landsat. *IEEE Transactions on Geoscience and Remote Sensing*, 62, pp. 1-10. https://doi.org/10.1109/TGRS.2024.3427836

15. Pahlevan, N., Mangin, A., Balasubramanian, S.V., Smith, B., Alikas, K., Arai, K., Barbosa, C., Bélanger, S., Binding, C. [et al.], 2021. ACIX-Aqua: A Global Assessment of Atmospheric Correction Methods for Landsat-8 and Sentinel-2 over Lakes, Rivers, and Coastal Waters. *Remote Sensing of Environment*, 258, 112366. https://doi.org/10.1016/j.rse.2021.112366

16. Wang, M., ed., 2010. Atmospheric Correction for Remotely-Sensed Ocean-Colour Products. *Reports of the International Ocean-Colour Coordinating Group*, No. 10. Dartmouth, NS: IOCCG, 78 p. https://doi.org/10.25607/OBP-101

17. Gordon, H.R. and Wang, M., 1994. Influence of Oceanic Whitecaps on Atmospheric Correction of Ocean-Color Sensors. *Applied Optics*, 33(33), pp. 7754-7763. https://doi.org/10.1364/AO.33.007754

18. Shybanov, E.B. and Papkova, A.S., 2022. Algorithm for Additional Correction of Remote Sensing Reflectance in the Presence of Absorbing Aerosol: Case Study. *Physical Oceanography*, 29(6), pp. 688-706. https://doi.org/10.22449/1573-160X-2022-6-688-706

19. Shybanov, E.B. and Papkova, A.S., 2025. A New Method for Retrieving Remote Sensing Reflectance from First-Level OLCI Satellite Data. *Russian Journal of Earth Sciences*, 25(3), pp. 1-19. https://doi.org/10.2205/2025ES001014

20. Shybanov, E.B., Papkova, A.S., Korchemkina, E.N. and Suslin, V.V., 2023. Blue Color Indices as a Reference for Remote Sensing of Black Sea Water. *Remote Sensing*, 15(14), 3658. https://doi.org/10.3390/rs15143658

21. Morel, A. and Gentili, B., 2009. The Dissolved Yellow Substance and the Shades of Blue in the Mediterranean Sea. *Biogeosciences*, 6(11), pp. 2625-2636. https://doi.org/10.5194/bg-6-2625-2009

22. Antoine, D., Hooker, S.B., Bélanger, S., Matsuoka, A. and Babin, M., 2013. Apparent Optical Properties of the Canadian Beaufort Sea - Part 1: Observational Overview and Water Column Relationships. *Biogeosciences*, 10(7), pp. 4493-4509. https://doi.org/10.5194/bg-10-4493-2013

23. Valente, A., Sathyendranath, S., Brotas, V., Groom, S., Grant, M., Taberner, M., Antoine, D., Arnone, R., Balch, W.M. [et al.], 2019. A Compilation of Global Bio-Optical In Situ Data for Ocean-Colour Satellite Applications - Version Two. *Earth System Science Data*, 11(3), pp. 1037-1068. https://doi.org/10.5194/essd-11-1037-2019

24. Lee, Z.P. and Hu, C., 2006. Global Distribution of Case-1 Waters: An Analysis from SeaWiFS Measurements. *Remote Sensing of Environment*, 101(2), pp. 270-276. https://doi.org/10.1016/j.rse.2005.11.008

25. Brewin, R.J.W., Raitsos, D.E., Dall'Olmo, G., Zarokanellos, N., Jackson, T., Racault, M.-F., Boss, E.S., Sathyendranath, S., Jones, B.H. [et al.], 2015. Regional Ocean-Colour Chlorophyll Algorithms for the Red Sea. *Remote Sensing of Environment*, 165, pp. 64-85. https://doi.org/10.1016/j.rse.2015.04.024

26. Cazzaniga, I. and Mélin, F., 2024. How Representative Are European AERONET-OC Sites of European Marine Waters? *Remote Sensing*, 16(10), 1793. https://doi.org/10.3390/rs16101793

27. Harmel, T., Gilerson, A., Tonizzo, A., Chowdhary, J., Weidemann, A., Arnone, R. and Ahmed, S., 2012. Polarization Impacts on the Water-Leaving Radiance Retrieval from Above-Water Radiometric Measurements. *Applied Optics*, 51(35), pp. 8324-8340. https://doi.org/10.1364/AO.51.008324

28. Zibordi, G., Mélin, F., Berthon, J.-F., Holben, B., Slutsker, I., Giles, D., D'Alimonte, D., Vandemark, D., Feng, H. [et al.], 2009. AERONET-OC: A Network for the Validation of Ocean Color Primary Products. *Journal of Atmospheric and Oceanic Technology*, 26(8), pp. 1634-1651. https://doi.org/10.1175/2009JTECHO654.1

29. Werdell, P.J., Fargion, G.S., McClain, C.R. and Bailey, S.W., 2002. *The SeaWiFS Bio-Optical Archive and Storage System (SeaBASS): Current Architecture and Implementation*. NASA/TM-2002-211617. Greenbelt, MD: NASA Goddard Space Flight Center, 45 p.

Submitted 23.01.2026; approved after review 09.04.2026;

accepted for publication 20.05.2026.

About the authors:

Evgeniy B. Shybanov, Leading Researcher, Marine Hydrophysical Institute of RAS (2 Kapitanskaya Str., Sevastopol, 299011, Russian Federation), DSc. (Phys.-Math.), **ORCID ID: 0000-0001-7943-305X**, **ResearcherID: ABB-9097-2021**, **Scopus Author ID: 6507075380**, **SPIN-code: 9906-9983**, e-shybanov@mail.ru

Anna S. Papkova, Junior Researcher, Marine Hydrophysical Institute of RAS (2 Kapitanskaya Str., Sevastopol, 299011, Russian Federation), CSc. (Phys.-Math.), **Scopus Author ID: 57203015832, WoS ResearcherID: AAP-3248-2020**, **SPIN-code: 1683-7685,** hanna.papkova@gmail.com

Contribution of the co-authors:

Evgeniy B. Shybanov – conceptualization and curation, methodology, data collection, investigation, visualization, preparatory drafting

Anna S. Papkova – methodology, investigation, data collection, formal analysis, visualization, preparatory drafting, review and editing

The authors have read and approved the final manuscript.
The authors declare that they have no conflict of interest.